Validation and Sensitivities of Frontal Clouds Simulated by the ECMWF Model

STEPHEN A. KLEIN

NOAA/Geophysical Fluid Dynamics Laboratory, Princeton University, Princeton, New Jersey

CHRISTIAN JAKOB

European Centre for Medium-Range Weather Forecasts, Reading, United Kingdom

(Manuscript received 9 July 1998, in final form 11 September 1998)

ABSTRACT

Clouds simulated by the European Centre for Medium-Range Weather Forecasts (ECMWF) model are composited to derive the typical organization of clouds surrounding a midlatitude baroclinic system. Comparison of this composite of about 200 cyclones with that based on satellite data reveals that the ECMWF model quite accurately simulates the general positioning of clouds relative to a low pressure center. However, the optical depths of the model's high/low clouds are too small/large relative to the satellite observations, and the model lacks the midlevel topped clouds observed to the west of the surface cold front.

Sensitivity studies with the ECMWF model reveal that the error in high-cloud optical depths is more sensitive to the assumptions applied to the ice microphysics than to the inclusion of cloud advection or a change of horizontal resolution from 0.5625° to 1.69° lat. This reflects the fact that in the ECMWF model gravitational settling is the most rapid process controlling the abundance of ice in the high clouds of midlatitude cyclones. These results underscore the need for careful evaluation of the parameterizations of microphysics and radiative properties applied to ice in large-scale models.

1. Introduction

Traditional methods of validation of clouds in large-scale models use monthly mean fields and their annual or interannual variability. This is natural since observations of clouds whether from the surface or by satellite have irregular space–time sampling such that only by averaging data over a period of time is it possible to discern the large-scale patterns of clouds that can be compared to a model. However, this method has a very serious drawback in that attribution of the causes of discrepancy between model and observations becomes a very difficult task, even if one assumes the observations are perfect. For example, if a large-scale model fails to produce enough clouds in a certain geographical region is that the fault of the cloud parameterization? Could it not also be due to a poor simulation of the large-scale circulation and its moisture transport? Or could it be due to feedbacks between the large-scale circulation and the cloud parameterization?

Clouds have lifetimes of minutes or hours to at most a few days. Consequently it is appropriate to examine cloud-related processes on these timescales to try to discern shortcomings in model simulations of clouds. A constraint on validation of shorter-term cloud variability has been the difficulty in accessing observations of clouds at timescales finer than monthly means. Recent efforts by both satellite and surface observation groups have greatly remedied this problem. For example, the International Satellite Cloud Climatology Project (ISCCP; Rossow and Schiffer 1991) provides 3-hourly resolution to the statistics of cloud properties (cloud fraction, cloud optical depth, cloud-top altitude) for 280 km $\times$ 280 km regions and to pixel-level results (sampled in space to 30-km resolution). A similar effort to process the observations of clouds recorded by observers at the surface (Hahn et al. 1996) provides access to the individual synoptic reports at both land stations and ships of opportunity. The potential research use of these datasets is immense.

Lau and Crane (1995, 1997, hereafter LC95 and LC97) examined both these datasets to provide a composite view of the synoptic organization of clouds around midlatitude and tropical weather systems. Their composites for the midlatitude weather systems display many of the features that have been traditionally identified by satellite analysis of frontal clouds (e.g., Browning 1990). In this work, the ability of the forecast model of the European Centre for Medium-Range Weather

Corresponding author address: Stephen A. Klein, NOAA/Geophysical Fluid Dynamics Laboratory, Princeton University Forrestal Campus, US Route 1, P.O. Box 308, Princeton, NJ 08542.
E-mail: sak@gfdl.gov

Forecasts (ECMWF) to simulate the clouds associated with wintertime baroclinic systems in the northwestern Atlantic is evaluated by comparison to the composite of LC95 and LC97. A forecast model is a unique and very valuable tool for validating cloud parameterizations. This is because the model can be initialized with realistic temperature, wind, and humidity structures corresponding to the observations. Provided that both the data assimilation system and the forecast model are of good quality, short-term forecasts will produce realistic circulation and humidity patterns and one of the uncertainties in cloud simulations, the large-scale forcing of clouds, can be reduced. The clouds then simulated by the forecast can be time matched to those in the observations.

Here, time-matched ECMWF reanalysis cloud data (section 2) is composited following the procedures of LC95. After this validation in section 3 of the ECMWF model's composite, a subset of 10 cyclones is selected for sensitivity studies. With this subset of cyclones, 24-h forecasts are run to determine how the simulation of frontal clouds depends upon model horizontal resolution, advection of cloud variables (cloud ice/water content and fraction), the treatment of ice settling by the model, and the use of prognostic versus diagnostic cloud schemes. From these sensitivity tests presented in section 4 the roles of various processes in the simulation of frontal clouds can be gauged.

2. ECMWF reanalysis data and review of LC95 composite procedure

For the cyclone composite presented in section 3, ECMWF reanalysis (ERA) data are analyzed. The ERA project (Gibson et al. 1997) is a reanalysis project covering the years 1979 through the end of 1993. The reanalysis is performed with the ECMWF integrated forecasting system, which includes the ECMWF model at spectral resolution of T106 (equivalent to 1.1256° resolution) and a data assimilation that cycles every 6 h. The T106 model includes 31 vertical eta levels, a semi-Lagrangian advection scheme, and parameterized physics. Noteworthy is that the ERA is the only reanalysis project to use a prognostic cloud scheme (Tiedtke 1993). See Gibson et al. (1997) for further details.

It is important to recognize that no cloud information is used in the assimilation cycle. Instead, the initial conditions for the cloud variables (cloud fraction and cloud water/ice content) are taken to be the final values from the previous 6-h forecast. Obviously this creates an initial imbalance at the starting time of each forecast with the analyzed temperature and humidity fields, which have been changed by the assimilation cycle from their final values in the previous 6-h forecast. However, with nonzero initial cloud fields, spinup times for the cloud variables are only a few time steps [see Fig. 2 of Jakob (1999)]. Hence, the balance between the cloud variables and the rest of the model is well established 18–24 h into integration from an analysis. Consequently, the clouds (and other prognostic variables) analyzed in this paper are taken from 24-h forecasts started from an analysis. For example, to examine the clouds of the ECMWF model for 1200 UTC 10 January 1985, the cloud variables from a 24-h forecast, which begins at 1200 UTC 9 January 1985 are analyzed. For a discussion of some general aspects of the performance of the cloud scheme in ERA see Jakob (1999).

TABLE 1. Classification of cloud types by range in cloud-top pressure, p_{ct}, and optical depth, τ. This classification scheme is identical to that of Rossow et al. (1991) with the exception that ECMWF clouds with $\tau \leq 0.1$ are not counted. This minimum τ was applied to the ECMWF clouds to mimic the fact that ISCCP has difficulty detecting clouds with optical thicknesses less than 0.1 (Jin et al. 1996).

Cloud type name	p_{ct} range (hPa)	τ range
Low-top thin	$680 < p_{ct}$	$0.1 < \tau \leq 3.6$
Low-top thick	$680 < p_{ct}$	$3.6 < \tau$
Middle-top thin	$440 < p_{ct} \leq 680$	$0.1 < \tau \leq 9.4$
Middle-top thick	$440 < p_{ct} \leq 680$	$9.4 < \tau$
High-top thin	$310 < p_{ct} \leq 440$	$0.1 < \tau \leq 3.6$
	$50 < p_{ct} \leq 310$	$0.1 < \tau \leq 9.4$
High-top medium	$310 < p_{ct} \leq 440$	$3.6 < \tau \leq 23$
	$50 < p_{ct} \leq 310$	$9.4 < \tau \leq 23$
High-top thick	$50 < p_{ct} \leq 440$	$23 < \tau$

To compare ERA cloud data to the LC95 composite of ISCCP satellite data, pseudosatellite observations of the model clouds are created (see the appendix for a full description of the method outlined below). That is, at every grid point in the model, account is taken of how a satellite would view an atmospheric column with physical properties specified by ERA. For example, only one cloud-top pressure, p_{ct}, can be assigned by ISCCP to each satellite pixel, and in the case of multilayer clouds this is usually the p_{ct} of the highest level cloud. In addition, the model's vertical profile of cloud fraction and its maximum-random overlap assumption are used to determine what fraction of the grid box is covered by clouds of a given range of p_{ct} and cloud optical depth, τ. This mimics the procedure of ISCCP to assign the fractional area covered by a given cloud type as the fraction of satellite pixels in a 280-km region that contain clouds with a range of p_{ct} and τ. See Table 1 for the various classifications of cloud types and their definitions in ranges of p_{ct} and τ. Finally two types of p_{ct} are derived from the model data. The first p_{ct} is the physical cloud-top pressure, that is, the midpoint pressure of the highest model level containing clouds. The second p_{ct} is an ''emissivity-adjusted'' cloud-top pressure. It accounts for the fact that in the case of thin (low emissivity) clouds overlying thick (high emissivity) clouds, the satellite is likely to overestimate p_{ct} and underestimate the physical cloud-top altitude. If τ of the column is low enough, ISCCP can use τ to estimate the emissivity of a single-layer cloud and make a smaller error in p_{ct}. However, this method does not work when τ is large and the upper levels of the cloud have low emissivity. The method to derive an emissivity-adjusted

p_{ct} follows ISCCP procedures and thus accounts for these satellite limitations.

According to the compositing procedure of LC95, a list of 63 key dates occurring during the months of October–March for each of 20 reference sites in the northwest Atlantic near 45°N, 50°W is created. The selection criteria for the key dates is that the daily-averaged ISCCP τ has a local (in time) maximum at the reference site. For each field variable being composited, the mean for the 5 days centered on the key date is subtracted from the data and the average value of this anomaly for the 63 dates is formed. This averaging creates 20 composite anomaly fields, one for each list of key dates. From these 20 fields, a single merged composite is made by averaging onto a grid of lat–long relative to the reference site of each of the 20 composite fields. This averaging preserves the relative horizontal positions of major cloud features associated with extratropical cyclones.

Because the period of the reanalysis project is contemporaneous with that of the ISCCP, this procedure can be applied to the 24-h forecasts from ERA using the exact same list of key dates and sites as in LC95. Because the selection criteria for dates depends solely on satellite observations and not on model data, there is no guarantee that the ERA forecasts will simulate clouds at the same positions and times as observed by the satellite. Thus by taking the list of key dates from LC95, a test is made of whether clouds from the 24-h forecasts correspond to those observed by satellite.

For their composite, LC95 use satellite data from any sunlit UTC hour over the domain of compositing. For the northwest Atlantic, local noon occurs near 1500 UTC; consequently, ERA data for 1200 UTC are used in this study. ERA data for 1500 UTC, although available as 3-h forecasts, are not used because of possible model spinup effects. Although there are theoretically 1260 ($=20 \times 63$) independent events in the composite of LC95, some key dates recur in the lists for different reference sites. In these instances, it is likely that the same cyclone is being entered in the lists of several reference sites because of the small distance between reference sites. Consideration of duplication of key dates and the average time it takes cyclones to cross the area covered by the reference sites yields an estimate of approximately 200 independent cyclones for the composite by LC95.

3. Comparison of ECMWF frontal clouds to satellite and surface observations

Figure 1a presents the composite of ISCCP clouds from LC95 superimposed on the composited anomalies in ERA 1000-hPa height and wind vectors. When viewing the LC95 composite, it is worthwhile to recall that LC95 use high-top optically thick clouds instead of dynamical fields as the basis for compositing. Consequently, the composite likely includes cyclones at different stages of their life cycle. Furthermore, the relative positioning of clouds to dynamical fields may vary between individual cyclones. Nonetheless, high-top clouds, plotted in various shades of red, predominate to the northeast of the low pressure center. (The term ''shield'' is used to describe this region of high-top clouds.) The optically thinnest of the high-top clouds are at the eastern edge of the shield in accordance with classical models of midlatitude cyclones (Bjerknes and Solberg 1922). Low-top clouds are present to the west of the low pressure center and to the east of the high-top cloud shield. However, surface observations indicate that clouds with low bases are also present in the regions of the cloud shield (LC97); the absence of low-top clouds in the shield region of the ISCCP composite arises either because high clouds obscure the satellite view of low clouds or because the clouds are geometrically tall with bases near the surface and tops high in the atmosphere. Middle-top thick clouds are present in a southwest to northeast band at the western edge of the cloud shield.

The composite of ECMWF clouds from ERA (Fig. 1b) contains many of the features of the ISCCP composite. A high-top cloud shield is present to the east of the surface low pressure center and has a similar shape to the satellite observations. Low-top clouds are simulated to the east and west of this shield. Although the ECMWF model simulates the general geographical locations of clouds well, noticeable errors exist in the optical thicknesses of simulated clouds. High-top thin clouds appear to be more abundant than observed at the eastern edge of the cloud shield. In addition, low-top clouds to the east of the cloud shield appear to be too optically thick.

The placement of middle-top thick clouds in the model is substantially different from the satellite composite. Contrary to the satellite observations, the model does not simulate any middle-top thick clouds in the southwest portion of the cyclone, a region that is often the site of ''cold-air outbreaks.'' In cold-air outbreaks, the tops of stratocumulus clouds grow in depth with distance downstream of the continents to reach middle levels of the troposphere. A possible explanation for the model error is that model underestimates the growth in the depth of the boundary layer in cold-air outbreaks. However, because this is the first study to identify this error, additional studies will be needed to verify this deficiency of the ERA forecasts. Interestingly, the positioning of the middle-top thick model clouds to the northwest of the low pressure center is in accord with the expected location of the ''cold conveyor belt'' (Carlson 1980), in which middle-top clouds form in westward-flowing ascending air to the north of the low pressure center. Only the western portion of this belt is visible to satellite because the air mass flows under the warm conveyor belt that forms the high-top cloud shield. Of course, not each of the approximately 200 cyclones in the composite will have these ''conveyor belts.''

Accounting for the difficulty satellites have in locating the physical top of clouds whose upper parts have partial emissivity alters the depiction of the ECMWF model clouds (Fig. 1c). Throughout much of the cloud shield, middle-top thick clouds are identified. This indicates that the high levels of the cloud shield are not emissive enough when using ISCCP's C-level radiation parameterization. This model deficiency suggests either (a) an underestimate of the ice water content of the uppermost parts of the cloud shield or (b) an incorrect parameterization of the ice particle size of the uppermost parts of the cloud shield. A similar deficiency was also identified by Jakob and Rizzi (1997), who showed that in simulating outgoing longwave radiation from the *TIROS-N* Operational Vertical Sounder (TOVS), the model overestimates the outgoing longwave radiation in the cloud shield of midlatitude cyclones. Jakob and Rizzi (1997) suggested that the most likely cause of the discrepancy was a model underestimate of the ice water content in the cloud shield. An underestimate of ice water content in the model's cirrus is also consistent with the results of a comparison of the ice water content inferred from radar data and that of a simulation by the ECMWF model of the First ISCCP Regional Experiment (FIRE) II Coffeyville, Kansas, case of 26 November 1991 (Stephens et al. 1998; Klein and Morcrette 1997). The sensitivity of this error to a change in ice microphysics is discussed in section 4c.

From synoptic observations of surface observers, LC97 composited categories of the reported weather type. Figure 2a displays their composite of precipitation types and fog superimposed on the composited anomalies in ERA 500-hPa vertical velocity. Anomalies in light and heavy rain occur in a southwest- to northeast-oriented band that lies in the western portion of the cloud shield. This rain pattern is roughly coincident with the region of ascent at 500 hPa and lies approximately 5° east of the 1000-hPa low pressure center and in the warm sector of the cyclone. Snow is reported to the northwest of the low pressure center and in the cold sector of the cyclone at 1000 hPa. Fog is reported in the eastern portion of the cloud shield and in a region of southerly 1000-hPa flow (i.e., warm advection). A composite of surface precipitation accumulated over the last 6 h of the ERA 24-h forecasts is superimposed on the composite of 24-h forecasts of 500-hPa vertical motion in Fig. 2b. (Instantaneous precipitation rates are not available from the ERA archive.) Stratiform precipitation is predominate in the center of the cyclone; however, the ratio of convective to stratiform precipitation increases in the southern portions of the cyclone. The peak anomaly in stratiform precipitation, 8 mm day^{-1}, occurs at $-2.5°$ relative lat, $-7.5°$ relative long, whereas the peak anomaly in convective precipitation, 4.3 mm day^{-1}, occurs at $-7.5°$ relative lat, $-7.5°$ relative long. Although the frequency of reports of heavy rain (Fig. 2a) and the model's convective precipitation (Fig. 2b) are both plotted with red pixels, it is not intended to imply a one-to-one correspondence between the two quantities. Likewise there is no implied correspondence between reports of light rain and the model's stratiform precipitation rate. As in the observations, snow is present in the northwestern portion of the cyclone; however, the model fog is incorrectly concentrated in the center of the precipitating region.

A potential cause of model error in cloud simulation could be an incorrect simulation of the large-scale dynamical flow. This can partially be checked by comparison of the dynamical fields from the 24-h forecasts to the analyses for the same time. Comparing the 1000-hPa height analysis in Fig. 1a to the 24-h forecast in Fig. 1b, the 24-h forecasts slightly underestimate the peak anomaly in the low pressure center (-64 m vs -60 m). This small error could arise because the model systematically underestimates the rate of cyclogenesis or because the model makes repeated errors in the track of cyclones. A larger discrepancy occurs in the 500-hPa vertical motion field. The peak anomaly in ascent is 0.24 Pa s^{-1} in the composite of 24-h forecasts (Fig. 2b), whereas it is 0.28 Pa s^{-1} in the analyses (Fig. 2a). To the extent that increased vertical motion encourages greater cloud optical thicknesses, the underestimate of vertical motion in the 24-h forecasts could partly contribute to an underestimate of the optical thickness of the cloud shield. However, as shown in a model sensitivity study below (section 4a), an increase in the vertical motion comparable to the difference between the 24-h forecasts and analyses would have a rather moderate impact on cloud water path. Overall, it is assumed that 24-h forecasts are reliable enough in an aggregate sense to be a reasonable portrait of the large-scale dynamics at a given time.

Figure 3 displays a cross section along the line AB in Fig. 1c for several model fields; the line AB is identical to that shown in LC95. The peak vertical motion (Fig. 3a) lies near 600 hPa somewhat lower and westward of the peak cloud fraction anomaly (Fig. 3b). The cloud fraction composite has a west to east tilt with altitude, which is consistent with the early models of warm fronts (Bjerknes and Solberg 1922). The tilt is also consistent with the common surface observation that as a cyclone approaches from the west, thin cirrus appears first, followed by a gradually lowering of cloud base and apparent thickening of the cloud. The composite anomaly of grid-mean ice/water content, l, normalized by the saturation value of specific humidity, (Fig. 3c) shows less west to east tilt with altitude than for cloud fraction. Peak values of normalized ice/water content are slightly above 0.02 or 2% of saturation.

LC95 also found an eastward displacement of the center of the cloud shield from the position of maximum vertical ascent (cf. Fig. 8 of LC95). The displacement in their figure ($\sim 5°$) is considerably greater than the displacement shown in Fig. 3 ($\sim 2°$). LC95 attribute the displacement of the cloud shield to the advection of clouds by the jet stream in the upper troposphere. The

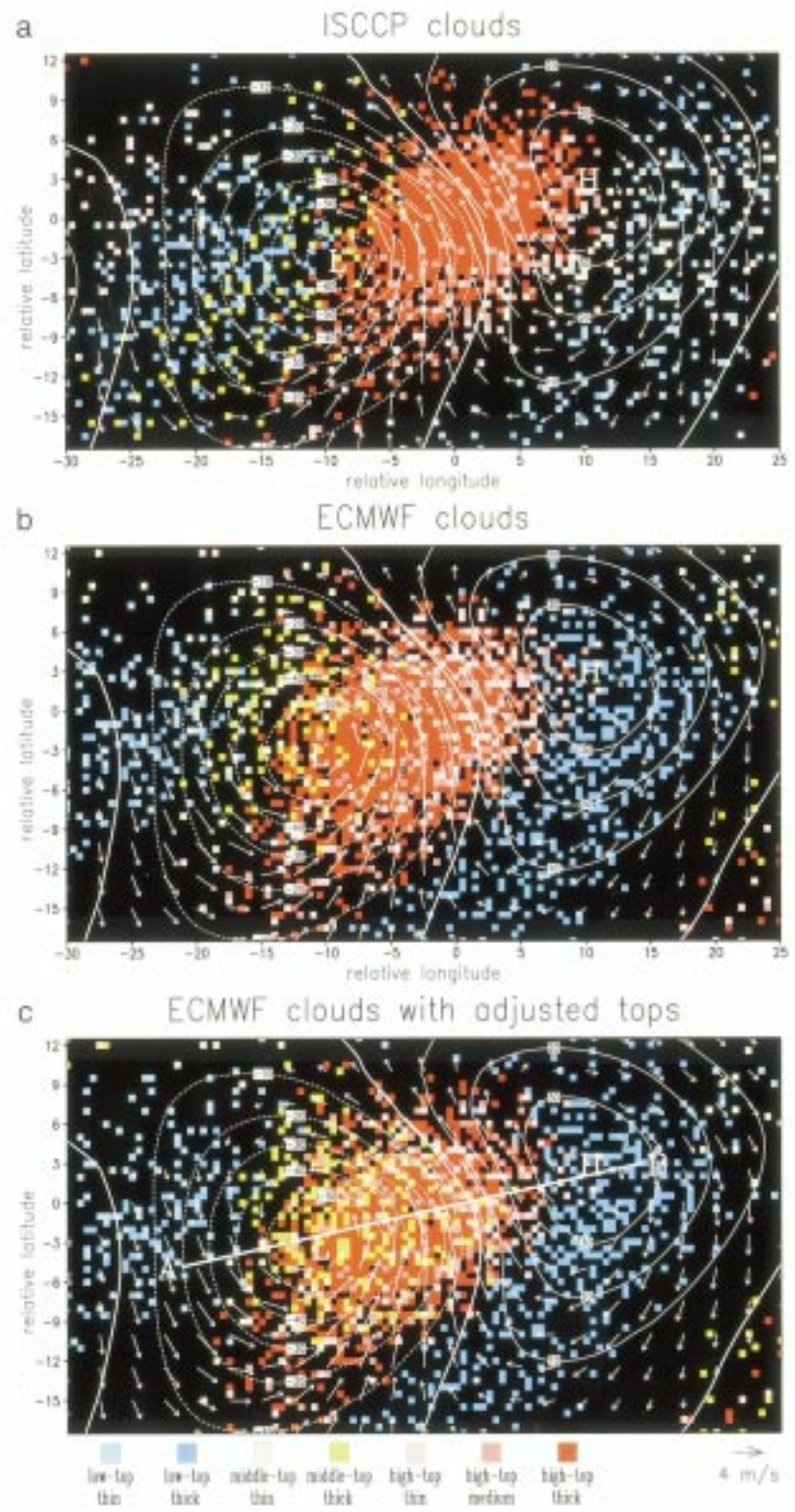

FIG. 1. (a) Distributions of 1000-hPa horizontal wind (arrows, see scale at bottom right) and geopotential height (contours, interval 10 m) from ERA analyses, and various cloud types (color pixels) from ISCCP observations as shown in LC95. The ordinate (abscissa) of the coordinate

ERA model does not include cloud advection, although temperature and vapor are advected by the semi-Lagrangian transport algorithm. This might suggest that the lack of cloud advection in ERA yields an incorrect displacement of the cloud shield from the position of greatest vertical ascent. However, the use of asynoptic datasets by LC95 may be the cause of the apparently large displacement in LC95. LC95 use ECMWF analyses that are the average of 0000 and 1200 UTC for a given date. However, the ISCCP data is from all sunlit hours on a given date. With local noon near 1500 UTC in the northwest Atlantic, there is effectively a 9-h time displacement between the cloud and dynamical fields in LC95. With the North Atlantic cyclones translating an average of 12–15 m s^{-1} in the eastward direction (LC95), the cloud field in LC95 is displaced 440 km or 5.5° (=13.5 m s^{-1} × 9 h) east of the analyses solely because of the use of asynoptic datasets. The use of asynoptic datasets is the likely explanation for why at the position of the low pressure center there are no high-top clouds (red pixels) in Fig. 6 of LC95 but there are some in the ERA composite (Fig. 1b). In addition, the slightly eastward shift of the ISCCP high-top clouds (Fig. 1a) relative to the ERA clouds (Fig. 1b) may be because the effective time of the ISCCP data is 1500 UTC, whereas the ERA clouds are from 1200 UTC. In summary, it is difficult to determine how much of the eastward displacement of the cloud shield from the position of greatest vertical motion seen in LC95 is real and possibly due to cloud advection and how much is not real because of the use of asynoptic datasets. The role of advection of clouds in the ECMWF model will be tested in section 4b.

4. Sensitivity studies

With a reasonable simulation of frontal clouds by the ECMWF model, it is possible to use the model to determine how the simulated clouds depend on model parameters and processes such as horizontal resolution, cloud advection, ice microphysics, and choice of cloud scheme. To this end, 10 key dates were selected at random from the list of 63 key dates at one of the 20 North Atlantic sites in LC95. For each date, a 24-h forecast was run using the ECMWF model as it was operational in spring 1997 but at T106 resolution. Although this model version differs from that used in ERA in several aspects, the only relevant difference for this study is the inclusion of cloud advection. The initial conditions for each forecast are provided from the ERA data. For these 10 forecasts, the composite procedure of LC95 was repeated. Because the LC95 composite averages variables that are departures from a 5-day mean centered on the key date, 40 additional forecasts were run so that departures from a 5-day mean could be calculated using forecasts with the same model. The composite based on these 50 forecasts will be designated the ''T106 control'' for sensitivity studies. For sensitivity studies, a selected parameter is changed and 50 forecasts are run with the altered model using the same dates and procedures as is used for the T106 control. The differences between composite variables of the perturbed model and the T106 control indicates the short-range sensitivity of a variable to the parameter change. The number of key dates selected, 10, appears to be sufficient to detect the signal of the sensitivity parameter from the noise due to differences between individual cyclones.

a. How do frontal clouds depend on the model's horizontal resolution?

To determine the sensitivity of the simulation to model resolution, the ECMWF model was run at T63 (~1.69°) and T213 (~0.5625°) resolution. (T213 is the 1997 resolution of ECMWF's operational 10-day forecast.) Although each model has 31 vertical levels, the time step of the model changes from 60 min for T63 to 45 min for the T106 control to 15 min for the T213. Although the model's horizontal resolution changes, all data displayed in figures is at 2.5° lat × 2.5° long resolution.

As horizontal resolution increases, cross sections through the cyclone composite indicate that the peaks in vertical motion increase in magnitude (Fig. 4). In the cross section, the peak ascent rate is near 0.21 Pa s^{-1} for T63 resolution but increases to 0.27 Pa s^{-1} for T213 resolution. The subsidence to the east and west of the cyclone increases in strength as well. This change in vertical velocity theoretically could increase the amounts of precipitation or clouds or both. For example, net condensation and cloud formation is parameterized directly in terms of the ascent rate in the prognostic cloud scheme [Eq. (21) of Tiedtke 1993]. However, Figs. 5 and 6 show that the anomalies in cloud fraction and cloud ice/water content increase only modestly. At T213, the west-to-east tilt of the cyclone is reduced.

←

FIG. 1. *(Continued)* system used here corresponds to latitudinal (longitudinal) displacements in degrees from the reference site. Inside each 2.5° × 2.5° grid box of this coordinate system, the presence and relative abundance of a certain cloud type is indicated by plotting a number of randomly scattered pixels with the color designated to the cloud species in questions (see legend at bottom and Table 1). Each pixel represents a 1% increment in cloud fraction; negative values of cloud fraction are not plotted. In this and all following figures, the composite data for all fields represent deviations from background levels estimated by averaging the values for the 5-day period entered on the key dates. (b) As in Fig. 1a but for cloud data and dynamical fields from the 24-h ERA forecasts. Clouds in this figure are classified by their physical cloud-top pressure. (c) As in Fig. 1b but using emissivity-adjusted cloud-top pressure. The line AB indicates the horizontal trace of the vertical cross section to be shown in several subsequent figures.

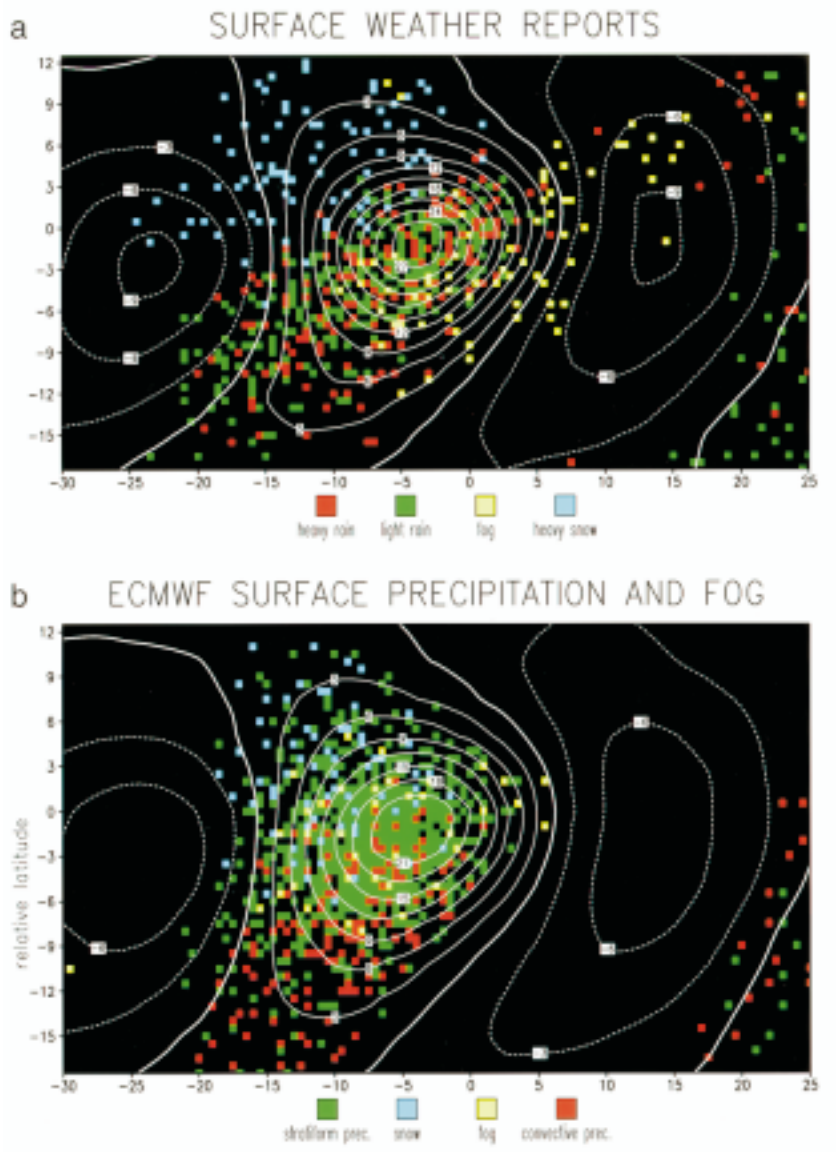

FIG. 2. (a) Composite patterns of the frequency of occurrence of selected surface weather types taken from LC97. The coordinate system used is identical to that of Fig. 1. In each 2.5° × 2.5° grid box, the presence and relative abundance of a given weather type are indicated by plotting randomly scattered pixels with a specific color (see legend at bottom), at the rate of one pixel for each percent increment in frequency of occurrence. Negative anomalies of weather types are not plotted. The composite anomaly pattern for 500-hPa vertical velocity, $-\omega$, from the ERA analyses is shown by contours with labels in units of 10^{-2} Pa s^{-1} and a contour interval of 3×10^{-2} Pa s^{-1}. Solid (dashed) contours indicate upward (downward) motion. (b) Composite patterns of the rates of various precipitation types and the frequency of occurrence of fog from the ERA forecasts. Precipitation rates shown include convective precipitation (sum of convective rain and convective snow), stratiform precipitation (sum of stratiform rain and stratiform snow), and snow (sum of convective and stratiform snow) plotted at the rate of 3 pixels per mm day^{-1} (see legend at bottom). The rate of precipitation is determined from the precipitation accumulated over the last 6 h of the 24-h ERA forecasts. Fog is determined to occur when the in-cloud ice/water content of the lowest model level, $l^{31}_{\text{in-cloud}}$, exceeds a threshold of 16 mg kg^{-1}. This threshold is used by Teixeira (1999) in analyzing fog in the ECMWF model and roughly corresponds to a visibility of 1 km according to Kunkel (1984). ERA fog is plotted at the rate of 1 pixel per percent cloud fraction. Negative precipitation and fog anomalies are not plotted. The composite anomaly pattern for 500-hPa vertical velocity from the 24-h ERA forecasts is plotted according to the style of Fig. 2a.

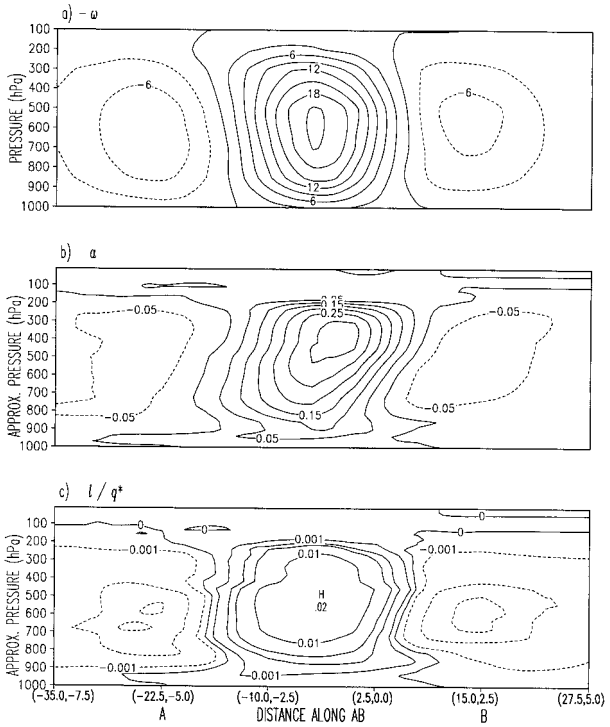

FIG. 3. Contours of (a) negative pressure velocity, $-\omega$ (interval: 3×10^{-2} Pa s^{-1}, positive values indicate rising motion); (b) cloud fraction, a (interval: 0.05, dimensionless); (c) grid-mean liquid water/ice content, l, normalized by the saturation value of specific humidity, q^* (logarithmic intervals at 0, ± 0.001, ± 0.003, ± 0.01, ± 0.03, ± 0.1, etc., dimensionless) in the vertical cross section taken along the line segment AB in Fig. 1c. The pairs of numbers at selected points along the x axis of (c) indicate the local abscissas and ordinates (in degrees of longitude and latitudes, respectively) with reference to the common coordinate system used in Figs. 1 and 2. The positions of the points A and B are indicated by letters beneath the abscissa in (c). Negative values can arise in (b) and (c) because the composite data for all fields represent deviations from background levels estimated by averaging the values for the 5-day period entered on the key dates.

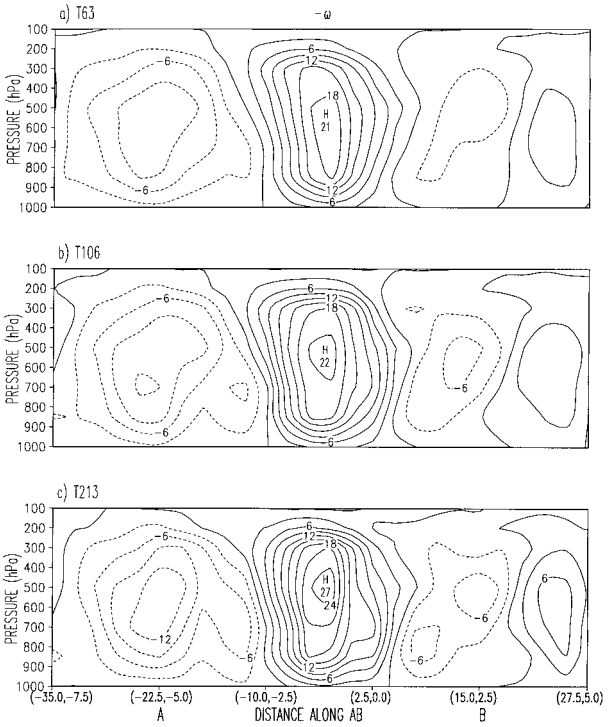

FIG. 4. Contours of negative pressure velocity, $-\omega$ (interval: 3×10^{-2} Pa s^{-1}, positive values indicate rising motion) for the ECMWF model at a horizontal resolution of (a) T63, (b) T106, and (c) T213 in a vertical cross section taken along the line segment AB in Fig. 1c. The composite anomalies in these and all subsequent figures are based on only the 10 cyclones chosen for sensitivity studies.

In terms of cloud water path, the increase in cloud water path with horizontal resolution is stronger for the peak anomalies than area-averaged anomalies (Fig. 7). As horizontal resolution increases, the peak cloud water path anomaly increases 21%; however, the difference plots indicate there is significant regional cancellation with areas of positive and negative changes in cloud water path. Averaged over the area of the cloud shield (the region bounded by $-10°$ and 2.5° relative lat, $-7.5°$ and 2.5° relative long), the cloud water path anomaly increases only 15%, going from 134 g m^{-2} at T63 resolution to 155 g m^{-2} at T213 resolution. The increases in cloud water path in the cloud shield slightly reduce the abundance of high-top thin and high-top medium clouds in the eastern portion of the cloud shield (not shown). Thus the overabundance of high-top thin and medium clouds in the ERA composite would have been partially alleviated if the ERA were performed at a horizontal resolution of T213. A moderate increase in global mean cloud water path with an increase in horizontal resolution from T63 to T106 was also seen in 30-day integrations of the ECMWF model with the prognostic cloud scheme (Table 2 of Tiedtke 1993). As suspected, precipitation averaged over the area bounded by $-12.5°$ and 2.5° relative lat, $-15°$ and $-2.5°$ relative long increases 18% going from 3.13 mm day^{-1} at T63 to 3.76 mm day^{-1} at T213.

b. How do frontal clouds depend on advection of clouds?

The advection of clouds by the large-scale dynamics is a process that is not always included in GCM simulations. This is due to the difficulty of avoiding spurious negatives in advecting positive-definite fields with strong horizontal gradients. Fortunately, models have not shown a strong sensitivity of the monthly mean cloud or radiation budget fields to the inclusion of cloud advection (Fowler and Randall 1996). How important cloud advection is for the representation of synoptic cloud features is an interesting question.

The T106 control runs include cloud advection, consequently, runs were made in which the semi-Lagrangian advection scheme transported only water vapor and temperature and not cloud fraction and ice/water content. Figures 8 and 9 indicate a moderate sensitivity of

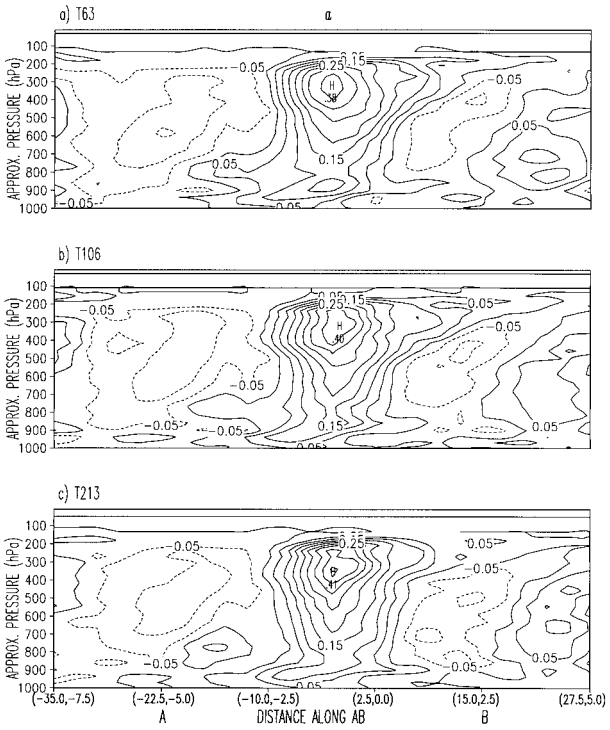

FIG. 5. As in Fig. 4 but for cloud fraction (interval: 0.05, dimensionless).

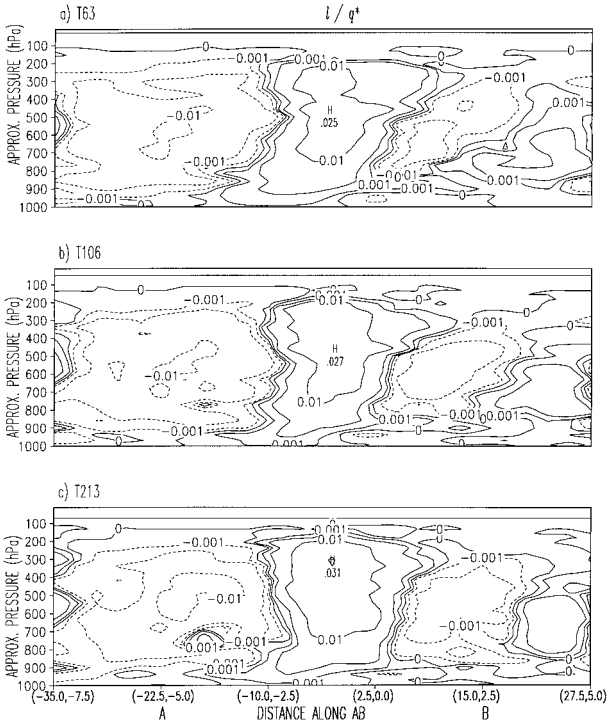

FIG. 6. As in Fig. 4 but for grid-mean liquid water/ice content normalized by the saturation value of specific humidity (logarithmic intervals at 0, ±0.001, ±0.003, ±0.01, ±0.03, ±0.1, etc., dimensionless).

the simulated cloud fraction and ice/water content field to the inclusion of cloud advection. Including cloud advection increases/decreases the cloud fraction and ice/water content on the east/west side of the cyclone consistent with westerly advection by the jet stream (wind cross section not shown). Unexpectedly, the greatest effect is in the lower troposphere, although the jet stream is strongest in the upper troposphere. In terms of cloud water path (Fig. 10) advection increases the cloud water path in the eastern portion of the cloud shield, but this is compensated by decreases elsewhere. Averaged over the area of the cloud shield (the region bounded by $-10°$ and 2.5° relative lat, $-7.5°$ and 2.5° relative long), the cloud water path anomaly is slightly greater in the run with cloud advection (143 g m^{-2} vs 132 g m^{-2}).

To understand the moderate sensitivity to cloud advection consider the timescales for various processes to remove or add cloud ice/water content in the vicinity of the cloud shield (Table 2). For the scale of the cloud shield and the wind speeds simulated by the ECMWF T106 model, horizontal advection has a shorter timescale and thus is a more rapid process than vertical advection. Consequently it is expected that the effects of horizontal advection would dominate over vertical advection and this is in general accord with the results of Figs. 8 and 9. To understand why greater impact is seen in the lower troposphere, compare the advection timescales to the timescale of precipitation sinks. In the upper troposphere, the ECMWF model parameterizes the sink of ice due to ice crystal gravitational settling. This is a very rapid process; consequently ice cannot be transported far before settling out of the jet stream. In the lower troposphere, the sink of cloud water due to autoconversion acts over a longer timescale than ice settling (the effects of accretion may shorten this timescale somewhat). Although the horizontal advection timescale is longer in the lower troposphere, the ratio of horizontal advection to autoconversion in the lower troposphere is 35% of the ratio of horizontal advection to ice settling in the upper troposphere. From this argument, the impact of horizontal advection should be larger in the lower troposphere because horizontal advection is a more rapid process in the lower troposphere *relative* to the local precipitation sink. This argument could explain why the effects of horizontal advection are more pronounced in the lower troposphere (Figs. 8 and 9).

c. How does cirrus depend on microphysical assumptions?

At temperatures less than 250 K, the primary microphysical sink of ice crystals in the ECMWF model is gravitational settling. The mass-weighted fall speed of ice crystals, V_f, is parameterized as a function of the cloud ice content according to a formula similar to that of Heymsfield and Donner (1990). All ice that settles

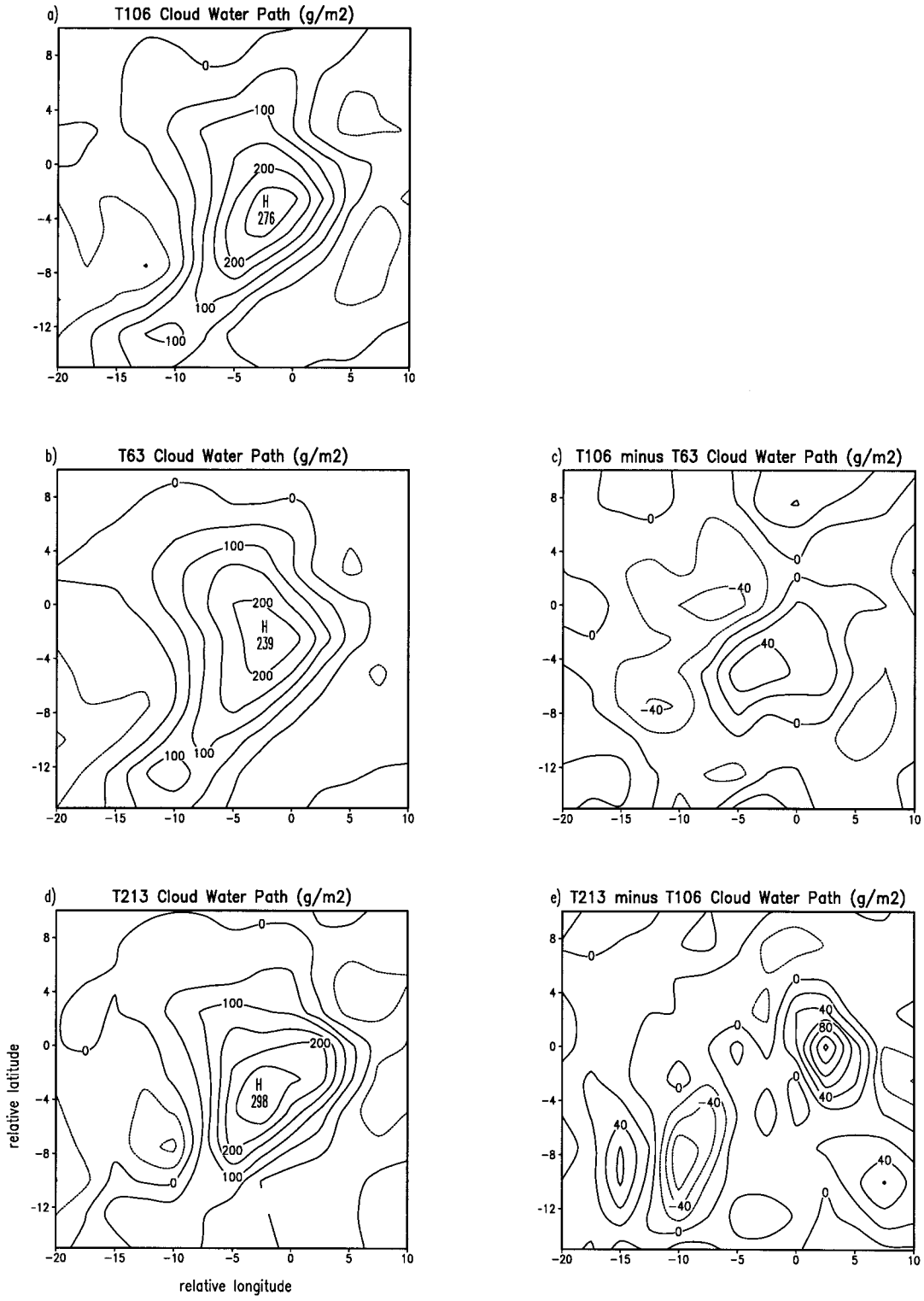

FIG. 7. Composite anomalies in cloud water path for (a) the T106 control simulation, (b) the T63 simulation, (c) the difference between (b) and (a), (d) the T213 simulation, and (e) the difference between (d) and (a). The ordinate (abscissa) of the coordinate system used here corresponds to latitudinal (longitudinal) displacements from the reference site. In (a), (b), and (d) the contour interval is 50 g m^{-2}, and the peak value is indicated by the letter ''H'' with the value printed beneath. In (c) and (e) the contour interval is 20 g m^{-2}. Negative values are indicated by dashed lines.

TABLE 2. Timescales associated with sources and sinks of cloud ice/water content, l, in the region of the cloud shield. Here ΔX is the horizontal scale of the cloud shield, approximately 500 km and U is the zonal wind speed taken as 20 m s^{-1} in the lower troposphere and 40 m s^{-1} in the upper troposphere. The pressure thickness scale, ΔP, is chosen as the scale height pressure for water vapor, approximately 100 hPa in the middle troposphere. This value of ΔP is selected because cloud ice/water content is a nearly constant fraction of the saturation specific humidity of water vapor, q^* (Fig. 6b). Here ω is the vertical pressure velocity, 0.2 Pa s^{-1}, c_o is the autoconversion rate for liquid, 10^4 s^{-1}, Δp is the pressure thickness of vertical levels, 40 hPa, ρ is the air density, g is the gravitational acceleration, and V_f is the fall speed of ice crystals, 0.5 m s^{-1}. The pressure thickness for ice settling is chosen to be that of a single model level because all ice that settles through the base of *each* model level in a single time step is converted to snow. The timescale for condensation was calculated at a pressure of 500 hPa, a temperature of 260 K, a vertical velocity of 0.2 Pa s^{-1}, and l/q^* of 0.02.

Process	Scaling term	Timescale (h)
Horizontal advection	$\Delta X/U$	6.9 (lower tropo.) 3.5 (upper tropo.)
Vertical advection	$\Delta P/\omega$	13.9
Liquid autoconversion	c_o^{-1}	2.8
Ice settling	$\Delta p/\rho g V$	0.5
Condensation	$l/[\omega(\partial q^*/\partial p)]$	0.4

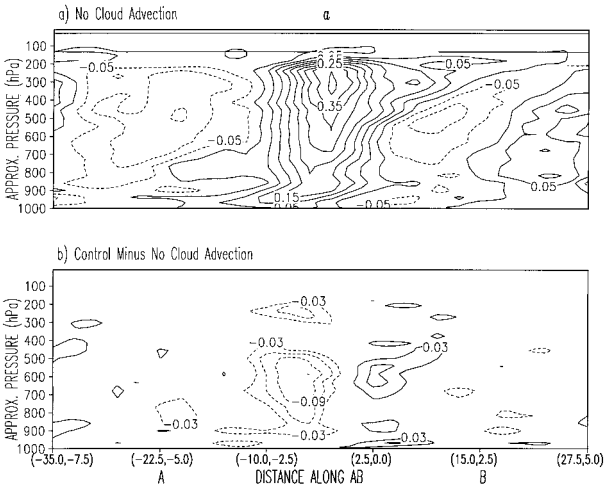

FIG. 8. Cross sections of cloud fraction (interval: 0.05, dimensionless) for (a) the T106 model without advection of cloud variable (fraction and ice/water content), and (b) the difference between (a) and the T106 control, which includes cloud advection. In (b), the difference is computed as the T106 control minus the T106 model without cloud advection. The cross section for the T106 control is shown in Fig. 5b. The cross section is taken along the line segment AB in Fig. 1c.

out of a layer is considered to be snow and thus enters the diagnostic snow flux. In December 1997 a change to this assumption was implemented into the operational model whereby ice settling out of a layer is considered to be a source of ice for the layer below if the layer below is cloudy. If the layer below is clear than the settling ice enters the snow flux. The difference is that crystals settling through a multilevel cloud are considered to be ice, whose radiative effects are included in the radiative transfer parameterization, instead of snow, whose radiative effects are assumed to be negligible and are not included in the radiative transfer parameterization.

The impact of this change upon the cloud ice/water content field is dramatic (Figs. 11–12). The peak anomaly in normalized cloud ice/water content quadruples (Fig. 11); and the integrated ice water path anomaly averaged over the area of the cloud shield (the region bounded by $-10°$ and 2.5° relative lat, $-7.5°$ and 2.5° relative long), increases from 46 g m^{-2} in the control to 87 g m^{-2} in the run with the ice fall change (Fig. 12). Since ice settling is the most rapid sink in the vicinity of the cyclone (Table 2), changes to the settling of ice crystals have a large impact on the simulated ice field.

One of the errors in the ERA composite was the apparent lack of emissivity of the high levels of the cloud shield. This error was partially attributed to an underestimate of ice content at high levels of the cloud shield. Since the change to ice microphysics dramatically alters the ice content in these regions, it is expected that this error would be reduced. Averaged over the center of the cloud shield (the region bounded by $-2.5°$ and 2.5° relative lat, $-2.5°$ and 0° relative long), the anomaly cloud amount of middle-top thick clouds (defined by their emissivity cloud-top pressures) decreases from 2.5% to -2.8%. In addition, the cloud amount anomalies of high-top thin and medium clouds also decrease from 3.9% to 2.9% and 4.3% to -0.1%, respectively, reducing their overabundance seen in the ERA composite. This would suggest that the implementation of this ice fall change into operations in December 1997 would alleviate the problems with the optical properties of the cloud shield. However, at the same time a change was made to increase the assumed particle size of ice-

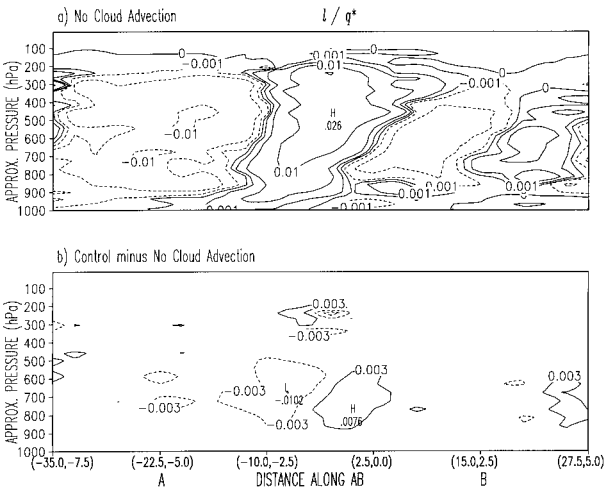

FIG. 9. As in Fig. 8 but for cloud ice/water content normalized by the saturation specific humidity (logarithmic intervals at: 0, ± 0.001, ± 0.003, dimensionless). The cross section for the T106 control is shown in Fig. 6b.

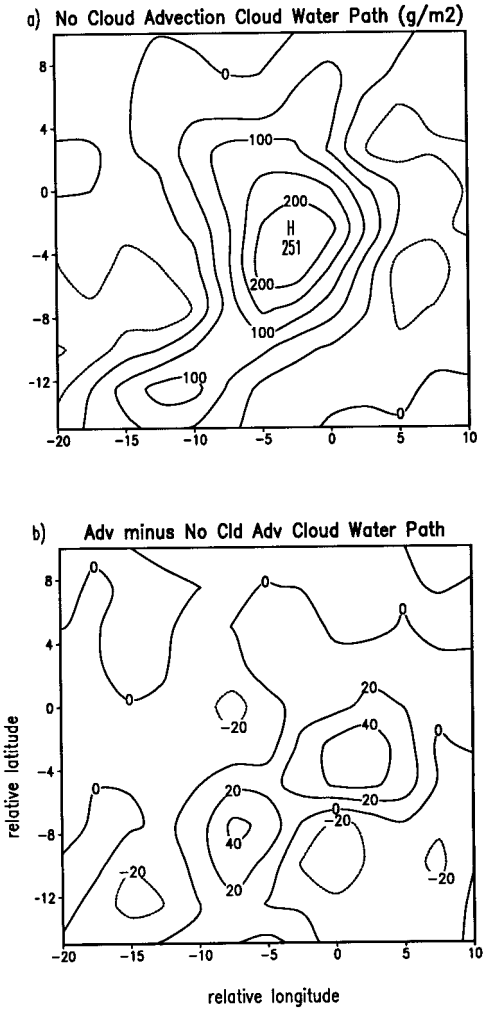

FIG. 10. (a) Composite anomalies in cloud water path for the T106 model without cloud advection, and (b) the difference between the cloud water path anomalies of the T106 control and the T106 model without cloud advection. The cloud water path anomalies for the T106 control are shown in Fig. 7a. Contour intervals and plotting conventions are as in Fig. 7.

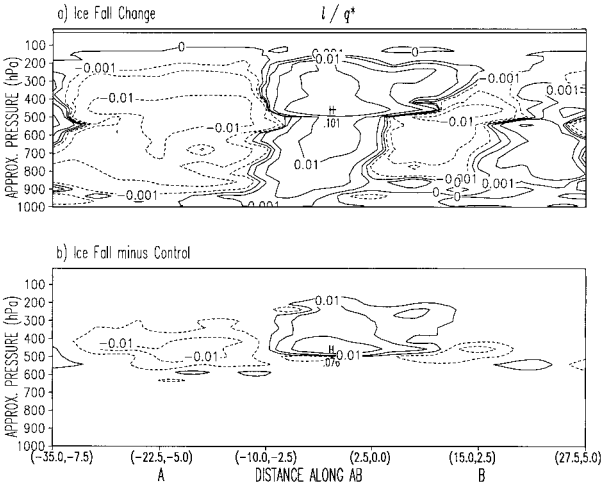

FIG. 11. Cross sections of cloud ice/water content anomalies normalized by the saturation specific humidity (logarithmic intervals at 0, ±0.001, ±0.003, ±0.01, ±0.03, ±0.1, etc., dimensionless) for (a) the T106 model with a change to the treatment of ice settling, and (c) the difference between (a) and T106 control. The difference is computed as the T106 model with the ice fall change minus the T106 control. The cross section for the T106 control is shown in Fig. 6b. The cross section is taken along the line segment AB in Fig. 1c.

crystals, which largely counteracted the change in ice water path as revealed in comparison between model outgoing longwave radiation and that deduced from TOVS (not shown). Consequently the optical properties of the cloud shield remains a concern.

d. How does the use of the prognostic cloud scheme alter the simulation of frontal clouds?

Virtually all GCMs have now implemented a budget equation for cloud ice/water content, that is, a ''prognostic'' cloud scheme (e.g., Sundquist 1988; Tiedtke 1993; Fowler and Randall 1996; Del Genio et al. 1996). These schemes replace the simpler diagnostic cloud schemes, which specify the occurrence and optical properties of clouds from instantaneous values of variables at the time of the radiation calculation. To examine how the cloud field depends on the cloud scheme, 24-h forecasts were run with the diagnostic cloud scheme, which was used previously in the ECMWF model (Slingo 1987).

The diagnostic cloud scheme is capable of reproducing the synoptic cloud organization (cf. Fig. 13b to Fig. 13a). The diagnostic cloud scheme simulates a cloud shield and the presence of low-topped clouds to the east and west of the cloud shield. The simulation of a cloud shield by the diagnostic cloud scheme is not surprising since these clouds form from saturation of air by the ascending motion, which is present regardless of the cloud scheme. Furthermore, the parameters used in the diagnostic scheme were chosen so that the model clouds would agree well with individual satellite pictures of frontal systems. Although the positioning of clouds differs little from the prognostic cloud scheme, the optical properties of the clouds can be different. The diagnostic cloud scheme simulates less ice in the tail of the cloud shield than the prognostic cloud scheme; however, it simulates more ice in the eastern edge of the shield. Cross sections illustrate larger differences in the cloud ice/water content composite than in the cloud fraction composite (not shown).

Although the differences between the diagnostic and prognostic cloud scheme appear small in the shown composite of North Atlantic winter cyclones, it is worthwhile noting that in general terms the prognostic cloud scheme outperforms the diagnostic one (Jakob 1994; Miller et al. 1995; Jakob 1999). A possible reason for the small differences found here is that many of the clouds found in extratropical cyclones form under the

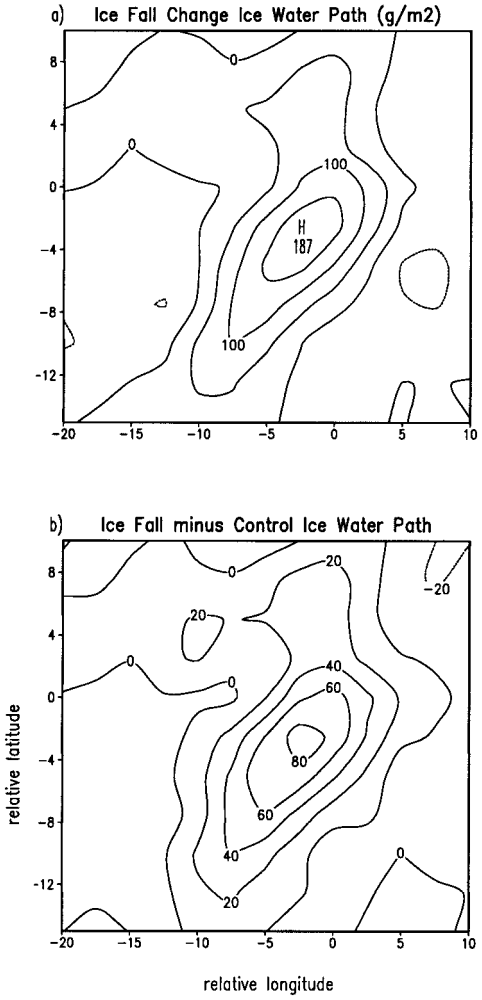

FIG. 12. (a) Composite anomalies in ice water path for the T106 model with the change to the treatment of ice settling, and (b) the difference between the ice water path anomalies of the model with the ice fall change and the T106 control. Contour intervals and plotting conventions are as in Fig. 7.

relatively strong forcing of large-scale (and hence model resolved) vertical motion and are therefore easier to predict even with simple schemes.

5. Conclusions

Contrary to traditional methods of cloud validation in large-scale models, observational data have been used to validate the simulation of clouds in a short-term phenomenon, a maritime midlatitude baroclinic cyclone. Knowledge gained about the behavior of the cloud scheme from this type of study can be used to direct future work to the specific synoptic environments that appear to be difficult to simulate. In the case of the ECMWF model, the simulation of high-top frontal clouds needs future work. Exercises of this sort should also be useful for defining deficiencies in lower-resolution climate models (although it is more difficult to access model data on short timescales from these models).

Since the *presence* of clouds in a cyclone depends strongly upon the large-scale circulation, which is reasonably simulated by a short-range forecast model, the model generally reproduces the positioning of clouds in cyclone. However, the *properties* of the clouds, which depend strongly on cloud microphysics and radiative properties, appear to be in error with respect to the satellite data. Two deficiencies of the simulation are discussed below.

First, the optical depths of the high-top clouds at the eastern edge of the cloud shield are too low. In addition, it appears that the high levels of the cloud shield are not emissive enough. These errors are not due to an incorrect physical location of the clouds in the model but due to an incorrect simulation of their physical properties. Further work on the microphysics and radiative properties of ice in the ECMWF model is needed to better simulate the optical properties of high-top frontal clouds.

Second, the optical thicknesses of low-top clouds to the east of the cloud shield appears to be overestimated by the ECMWF reanalysis relative to the satellite observations. In these regions, cloud fraction and cloud ice/water content are formed by detrainment of the shallow convection scheme or the stratocumulus scheme (Tiedtke 1993). Work in progress alters the assumptions of the physical properties of shallow cumuli detrainment, which should reduce both the cloud fraction and optical thickness of clouds formed in shallow convective regimes and perhaps reduce the error seen in the ERA composite (D. Gregory 1997, personal communication). This error is not affected by any of the sensitivity studies performed in this paper.

Sensitivity studies indicate that the properties of the cloud shield are more sensitive to microphysical assumptions than to model horizontal resolution or advection of cloud variables. The large sensitivity to ice microphysics indicates that the uncertainties that currently exist in the parameterization of ice microphysics (and radiative properties) for large-scale models need to be resolved. The relative insensitivity to model horizontal resolution occurs for model resolutions between T63 and T213, and may not be indicative of lower-resolution climate models in which the resolution is comparable to the Rossby radius of deformation. The relative insensitivity to cloud advection arises only because ice crystals settle out of the layer before they can be advected far horizontally. If the gravitational settling of ice crystals were less rapid, as might be suggested by the error in the optical properties of the cloud shield, the model clouds would be more sensitive to horizontal advection.

Clouds in midlatitude baroclinic systems are the subject of working group 3 of the Global Energy and Water Cycle Experiment's Cloud System Studies (Stewart et al. 1998). It is intended that this study provide a context

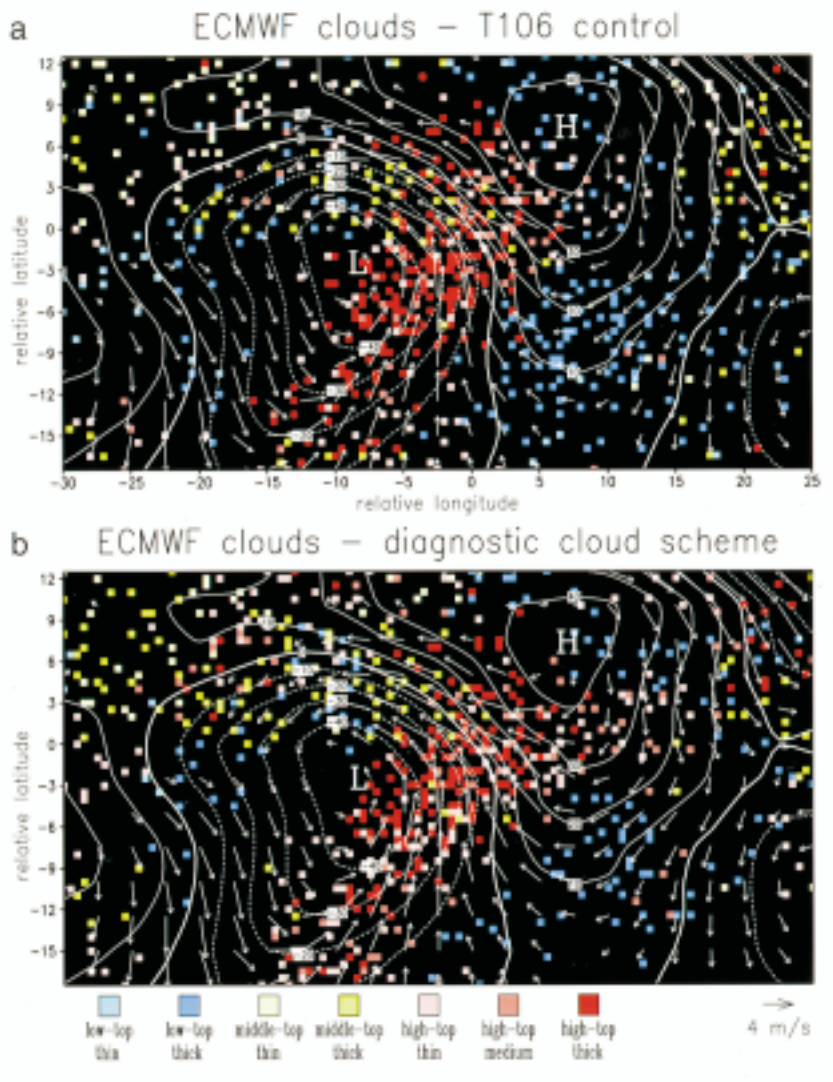

FIG. 13. As in Fig. 1c but for cloud data and dynamical fields from the 24-h forecasts of (a) the T106 control and (b) the T106 model run with the diagnostic cloud scheme. Each pixel represents a 4% increment in cloud fraction; negative values of cloud fraction are not plotted. Clouds in this figure are classified by their emissivity-adjusted cloud-top pressure.

for the issues of difficulty in GCM simulation of cyclone clouds. For the ECMWF model, efforts should be focused on properly defining the microphysical properties of the cloud shield that accompanies well-developed baroclinic systems, in particular, the microphysics and radiative properties of upper-tropospheric ice clouds need detailed attention.

Acknowledgments. The first author expresses his thanks to Tony Hollingsworth, Martin Miller, and Anton Beljaars, who made possible a visit to the ECMWF of 8 months by the first author. The first author hopes that ECMWF has benefited as much as the first author has from this visit. Assistance in performing the model experiments provided by Nils Wedi and David Dent of ECMWF is kindly acknowledged. Mark Crane of GFDL kindly supplied his plotting programs and data from the LC95 and LC97 studies. Comments on the manuscript by Anton Beljaars, Ngar-Cheung Lau, Martin Miller, and Brian Soden are appreciated. The speed with which the anonymous reviewers returned their comments to the editor is greatly appreciated.

APPENDIX

The Method of Simulation of ISCCP Cloud Data from ECMWF Model Data

Pseudosatellite data is produced by simulating the method by which a satellite would view an atmosphere

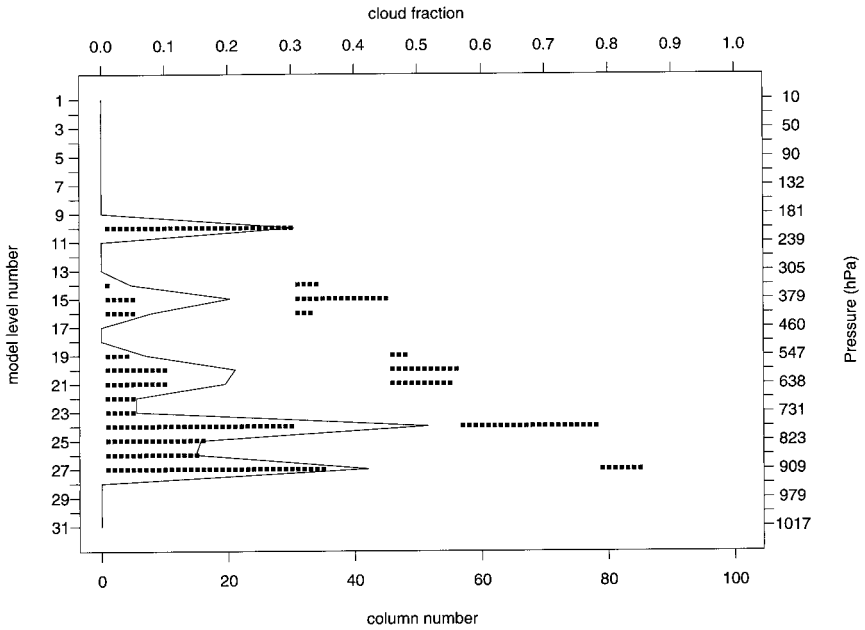

FIG. A1. The vertical profile of cloud fraction (thin line, scale at top) at a single instant and grid point from the ERA data. Superimposed on the figure is the subgrid distribution of clouds for the 100 subcolumns that result from the algorithm described in the appendix. The occurrence of a cloud at a given subcolumn and model level is indicated by a solid black square. The conversion of model level number to pressure is indicated by the scale at right.

that has the physical properties specified by the model. The complete ISCCP algorithm is not applied to the model data but account is taken of two important characteristics of satellite observations of clouds. The first is that satellites identify clouds by their tops and do not determine their bases or physical thicknesses. For example, if a high-level cloud overlies a low-level cloud, it will generally be identified as only a high-level cloud by a satellite. The second characteristic that affects satellite views of clouds is that satellites may underestimate the altitude of clouds with partial emissivity, especially if the partial emissivity cloud lies above an optically thick cloud. The method described below is similar to that used by Yu et al. (1996).

Every vertical level of a grid column of the model has the amount of liquid, ice, and the fraction of the grid box volume that contains cloud. The vertical profile of cloud amount together with the cloud overlap assumption provides information about what portion of clouds from each level contain no clouds above them and thus are visible by a satellite or which portion of clouds from each level are covered by clouds above and are not visible from space. To simulate the overlapping of clouds, each grid column of the model is subdivided into 100 subcolumns in which the cloud fraction is assigned to be zero or one at every model level. A sample vertical profile of cloud fraction from the ECMWF model and its possible distribution of cloudy and clear-sky subcolumns is shown in Fig. A1. To arrive at this distribution of cloudy and clear-sky subcolumns, several assumptions were made, the details of which are explained below.

First, it is assumed that clouds fill the grid box completely in the vertical; that is, the fraction of grid box volume that contains cloud is equal to the fraction of the horizontal area of a grid box that contains cloud. Although many clouds have thicknesses less than 500 m (Wang and Rossow 1995), this may not be too bad an approximation for the ECMWF model, which has 31 levels in the vertical with typical resolution of 40 hPa (about 400–700 m) in the middle and upper troposphere.

Second, at each level the specification of which subcolumns contain cloud is entirely consistent with the cloud overlap assumption used for the subgrid-scale flux calculations in the radiation scheme. The overlap assumption currently used in the ECMWF radiation scheme is that of maximum-random overlap (Geleyn and Hollingsworth 1979; Morcrette and Fouquart 1986). It can be described using the following equation, which specifies the total horizontal area, C^k, covered by clouds between the top of the atmosphere and a given model level k as

$$\frac{1 - C^k}{1 - C^{k-1}} = \frac{1 - \max(a^{k-1}, a^k)}{1 - \min(a^{k-1}, 1 - \delta)}, \qquad \text{(A1)}$$

where a^k is the cloud fraction of level k, $\delta = 10^{-6}$, and $k = 1$ for the top model level. Equation (A1) yields random overlap for clouds that do not occur in adjacent vertical levels but maximum overlap if clouds occur at

adjacent levels with cloud fraction monotonically increasing or decreasing with height. This equation is broadly consistent with the data on cloud overlap of Tian and Curry (1989). At each level, the number of subcolumns that contain cloud is equal to the nearest integer value of $100a^k$.

The use of (A1) provides a total cloud fraction, C^k, by applying it from the model top to level k given the distribution of clouds layer by layer. However, the knowledge of C^k and a^k alone is not sufficient to unambiguously assign the distribution of cloudy subcolumns. In level 15, the nine cloudy subcolumns, which fall in columns containing clouds at higher levels, could be placed in any of the first 34 subcolumns without violating (A1). Therefore, two additional assumptions are made: (i) in the spirit of maximum overlap for clouds in adjacent levels, clouds are assigned to those subcolumns that contain cloud in the layer immediately above in preference to those subcolumns that do not contain cloud in the layer immediately above but do have clouds higher in the same subcolumn, and (ii) the assignment of cloudy subcolumns at each level begins from the subcolumn farthest to the ''left'' that fulfills (i). Although (ii) is rather arbitrary, sensitivity tests revealed minimal sensitivity to this assumption.

The amount of liquid and ice at each level must be divided among the cloudy subcolumns of each level. For lack of a better method, each cloudy subcolumn is filled with the same amount of liquid and ice assuming a constant in-cloud water/ice content, l^k_{cld}, defined as

$$l^k_{\text{cld}} = l^k/a^k_{\text{int}}, \tag{A2}$$

where l^k is the grid-mean liquid water/ice content and a^k_{int} is a rounded cloud fraction calculated as the fraction of subcolumns at each level that contain cloud.

Consideration is then given to how a satellite would then detect a distribution of cloud tops and cloud optical depths from this allocation of clouds into subcolumns. The cloud optical depth, τ, for a given subcolumn is determined using the total liquid plus ice water path, WP in g m^{-2}, of the subcolumn by

$$\tau = 0.15893\text{WP}. \tag{A3}$$

Equation (A3) was used for the C level product of ISCCP, the satellite data used in the LC95 composite (Rossow et al. 1991). To calculate the pressure of the cloud top, p_{ct}, two methods are used. The first method is to merely assign p_{ct} as the midlevel pressure of the highest level with cloud for each subcolumn. This cloud top is the ''true'' or ''physical'' cloud-top pressure.

However, if the emissivity of the clouds' uppermost layers is less than unity, then the satellite will have difficulty detecting the true cloud-top pressure. If the subcolumn contains thin cirrus with no cloud beneath, ISCCP has a method to account for partial cloud emissivity to determine the true cloud-top pressure. However, if the partial emissivity cirrus is above an optically thick lower-level cloud or is part of a cloud whose lower layers have unit emissivity, then ISCCP will overestimate the cloud-top pressure (and thus underestimate its true altitude). An emissivity-adjusted cloud-top pressure is derived by crudely simulating the infrared water vapor window brightness temperature for each subcolumn and then following the procedures ISCCP would use to derive cloud-top pressure. The radiance at the top of the atmosphere, I, is the sum of the radiance emitted from each model level k multiplied by the transmittance, Tr, from level k to the top of the atmosphere plus the contribution of the surface emission:

$$I = \sum_{k=1}^{31} \text{Tr}^k \epsilon^k f\{T^k\} + \text{Tr}^{32} \epsilon^{\text{sfc}} f\{T^{\text{sfc}}\}, \tag{A4}$$

where ϵ^k is the emissivity of level k, and $f\{T^k\}$ represents a quantity linearly proportional to the radiation emitted by a blackbody at 11 μm:

$$f\{T^k\} = [\exp(1307.27/T^k) - 1]^{-1}, \tag{A5}$$

where T^k is the model temperature at level k. Within the atmosphere, the emissivity of level k depends on the occurrence of cloud and is derived from the visible optical depth that is due to cloud in level k (Rossow et al. 1991):

$$\epsilon^k = 1 - \exp(-\tau^k/2), \tag{A6}$$

where $\tau^k = 0.15893\text{WP}^k$ is the contribution to the cloud optical depth of the subcolumn from the cloud water path of level k, WP^k. The factor of 2 in (A6) is the factor to convert visible optical depths to infrared optical depths. For the surface an emissivity of 0.99 is used. The transmittance Tr from level k to the top of the atmosphere is given by the product of the transmissivities of each of the levels above:

$$\text{Tr}^k = \prod_{j=1}^{k-1} 1 - \epsilon^j \quad \text{with Tr}^1 = 1. \tag{A7}$$

Effects neglected by our crude model include the emission from the water vapor continuum, a proper treatment of the emission of the surface, the dependence of radiance on the zenith angle of the satellite, and the response function of the satellite.

Once the radiance at the top of the atmosphere, I, has been calculated for each subcolumn, consideration is given to how ISCCP would use this radiance to derive a cloud-top pressure. Regardless of the number of cloud layers, ISCCP interprets the radiance from each pixel in terms of a single cloud and retrieves only one cloud-top pressure. The emissivity of the cloud, ϵ^{cld}, is determined from the total optical depth of the subcolumn, τ:

$$\epsilon^{\text{cld}} = 1 - \exp(-\tau/2). \tag{A8}$$

The radiance at the top of the atmosphere, I, is assumed to be the sum of the emission from this single cloud and the portion of the emission from the surface that is transmitted through this single cloud:

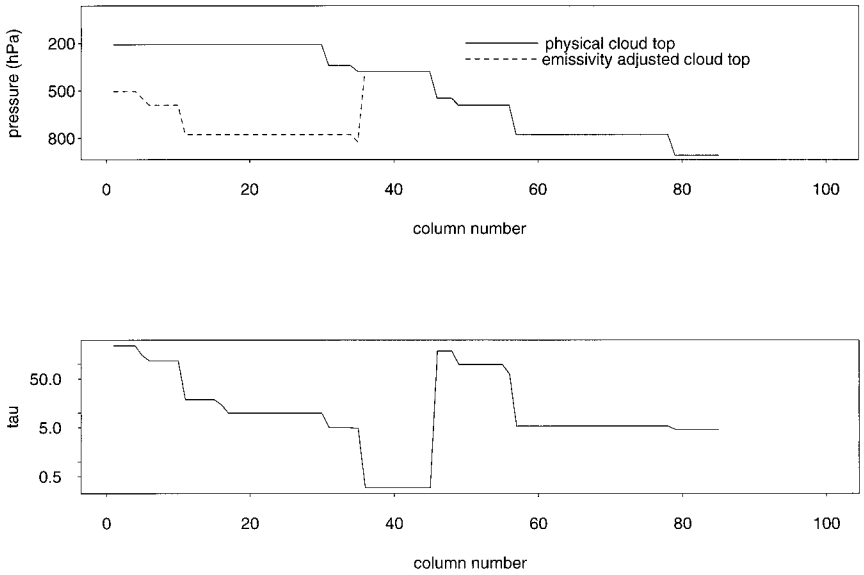

FIG. A2. (a) Simulated cloud-top pressure, p_{ct}, vs subcolumn for the cloud fraction profile shown in Fig. A1. The physical p_{ct} is indicated by the solid line, whereas the emissivity-adjusted p_{ct} is indicated by the dashed line where it differs from the physical p_{ct}. (b) Simulated cloud optical depth, τ, vs subcolumn for the cloud fraction profile shown in Fig. A1. Note that the ordinate is plotted on a logarithmic scale.

$$I = \epsilon^{\text{cld}} f\{T^{\text{cld}}\} + (1 - \epsilon^{\text{cld}})\epsilon^{\text{sfc}} f\{T^{\text{sfc}}\}. \quad \text{(A9)}$$

Then T^{cld} is varied until (A9) is satisfied. The emissivity-adjusted cloud-top pressure is then assigned to the pressure of the model level nearest the surface in which T^{cld} occurs.

The optical depths and cloud-top pressures derived by this method for each of the subcolumns of Fig. A1 is shown in Fig. A2. For subcolumns 1–30 the emissivity-adjusted cloud-top pressure is approximately the cloud-top pressure of the thicker lower cloud deck, and much lower in altitude than the physical cloud-top pressure. LC95 used the ISCCP C1 product, which reports the frequency of pixels in a 280 km × 280 km area containing clouds in certain ranges of optical depth and cloud-top pressure. To mimic the C1 product at every grid point of the ECMWF model, the fraction of subcolumns that contain clouds within the very same ranges of cloud-top pressures and visible optical depths is computed (Table 1). In this way an equivalence is made between the fractional areas covered by certain types of clouds as seen by the satellite and simulated from the model. In the example of Figs. A1 and A2, the frequency of high-top thick clouds and middle-top thick clouds is 0.1 and 0.11, respectively, when using the physical cloud-top pressure, but is 0.0 and 0.21 when using the emissivity-adjusted cloud-top pressure.

REFERENCES

Bjerknes, J., and H. Solberg, 1922: Life cycle of cyclones and the polar front theory of atmospheric circulation. *Geofys. Publ.,* **3,** 1–18.

Browning, K. A., 1990: Organization of clouds and precipitation in extratropical cyclones. *Extratropical Cyclones: The Erik Palmén Memorial Volume,* C. Newton and E. O. Holopainen, Eds., Amer. Meteor. Soc., 129–153.

Carlson, T., 1980: Airflow through mid-latitude cyclones and the comma cloud pattern. *Mon. Wea. Rev.,* **108,** 1498–1509.

Del Genio, A. D., M.-S. Yao, W. Kovari, and K. K.-W. Lo, 1996: A prognostic cloud water parameterization for global climate models. *J. Climate,* **9,** 270–304.

Fowler, L. D., and D. A. Randall, 1996: Liquid and ice cloud microphysics in the CSU general circulation model. Part III: Sensitivity to modelling assumptions. *J. Climate,* **9,** 561–586.

Geleyn, J.-F., and A. Hollingsworth, 1979: An economical analytical method for the computation of the interaction between scattering and line absorption of radiation. *Beitr. Phys. Atmos.,* **52,** 1–16.

Gibson, J. K., P. Kållberg, S. Uppala, A. Hernandez, A. Nomura, and E. Serrano, 1997: ECMWF Re-analysis Project report series: 1. ERA Description. ECMWF, 72 pp. [Available from European Centre for Medium-Range Weather Forecasts, Shinfield Park, Reading, Berkshire, RG2 9AX, United Kingdom.]

Hahn, C. J., S. G. Warren, and J. London, 1996: Edited synoptic cloud reports from ships and land stations over the globe, 1982–1991. DOE Rep. NDP026B, 45 pp. [Available from Carbon Dioxide Information Analysis Center, Oak Ridge National Laboratory, P.O. Box 2008, Oak Ridge, TN 37831-6335.]

Heymsfield, A. J., and L. J. Donner, 1990: A scheme for parameterizing ice-cloud water content in general circulation models. *J. Atmos. Sci.,* **47,** 1865–1877.

Jakob, C., 1994: The impact of the new cloud scheme on ECMWF's integrated forecasting system (IFS). *Proc. ECMWF/GEWEX Workshop on Modelling, Validation and Assimilation of Clouds,* Reading, United Kingdom, ECMWF, 277–294.

——, 1999: Cloud cover in the ECMWF reanalysis. *J. Climate,* **12,** 947–959.

——, and R. Rizzi, 1997: Evaluation of model OLR in cloudy regions using TOVS-1B data. *Proc. Ninth Int. TOVS Study Conf.,* Igls, Austria, NESDIS/EUMETSAT, 197–206.

Jin, Y., W. B. Rossow, and D. Wylie, 1996: Comparison of the cli-

matologies of high-level clouds from HIRS and ISCCP. *J. Climate,* **9,** 2850–2879.

Klein, S. A., and J. J. Morcrette, 1997: Simulation of a cirrus cloud observed during the FIRE-II field experiment. ECMWF Research Department memorandum R46.2/SK/JAM/82, 16 pp. [Available from European Centre for Medium-Range Weather Forecasts, Shinfield Park, Reading, Berkshire, RG2 9AX, United Kingdom.]

Kunkel, B. A., 1984: Parameterization of droplet terminal velocity and extinction coefficient in fog models. *J. Climate Appl. Meteor,* **23,** 34–41.

Lau, N. C., and M. W. Crane, 1995: A satellite view of the synoptic-scale organization of cloud properties in midlatitude and tropical circulation systems. *Mon. Wea. Rev.,* **123,** 1984–2006.

——, and ——, 1997: Comparing satellite and surface observations of cloud patterns in synoptic-scale circulation systems. *Mon. Wea. Rev.,* **125,** 3172–3189.

Miller, M. J., M. Hortal, and C. Jakob, 1995: A major operational model change. *ECMWF Newslett.,* **70,** 2–8.

Morcrette, J.-J., and Y. Fouquart, 1986: The overlapping of cloud layers in shortwave radiation parameterizations. *J. Atmos. Sci.,* **43,** 321–328.

Rossow, W. B., and R. A. Schiffer, 1991: International Satellite Cloud Climatology Project (ISCCP) cloud data products. *Bull. Amer. Meteor. Soc.,* **72,** 2–20.

——, L. C. Garder, P. J. Lu, and A. W. Walker, 1991: International Satellite Cloud Climatology Project (ISCCP) documentation of cloud data. WMO/TD-No. 266, World Meteorological Organization, Geneva, Switzerland, 76 pp. plus 3 appendixes.

Slingo, J. M., 1987: The development and verification of a cloud prediction scheme for the ECMWF model. *Quart. J. Roy. Meteor. Soc.,* **113,** 899–927.

Stephens, G. L., C. Jakob, and M. Miller, 1998: Atmospheric ice—A major gap in understanding the effects of clouds on climate. *GEWEX Newslett.,* **8** (1), 20 pp.

Stewart, R. E., K. K. Szeto, R. F. Reinking, S. A. Clough, and S. P. Ballard, 1998: Midlatitude cyclonic cloud systems and their features affecting large-scale and climate. *Rev. Geophys.,* **36,** 245–273.

Sundquist, H., 1988: Parameterization of condensation and associated clouds in models for weather prediction and general circulation simulation. *Physically-Based Modelling and Simulation of Climate and Climate Change,* M. E. Schlesinger, Ed., Kluwer, 433–461.

Teixeira, J., 1999: Simulation of fog with the ECMWF prognostic cloud scheme. *Quart. J. Roy. Meteor. Soc.,* **125,** 529–552.

Tian, L., and J. A. Curry, 1989: Cloud overlap statistics. *J. Geophys. Res.,* **94,** 9925–9935.

Tiedtke, M., 1993: Representation of clouds in large-scale models. *Mon. Wea. Rev.,* **121,** 3040–3061.

Wang, J., and W. B. Rossow, 1995: Determination of cloud vertical structure from upper-air observations. *J. Appl. Meteor.,* **34,** 2243–2258.

Yu, W., M. Doutriaux, G. Sèze, H. Le Treut, and M. Desbois, 1996: A methodology study of the validation of clouds in GCMs using ISCCP satellite observations. *Climate Dyn.,* **12,** 389–401.